Inorganic Chemistry Communications 183 (2026) 115790

Contents lists available at ScienceDirect

Inorganic Chemistry Communications

journal homepage: www.elsevier.com/locate/inoche

Research Article

Design of innovative nitrogen-doped carbon quantum dots integrated with magnetic nanocomposite barium ferrite for enhanced supercapacitors electrode performance

Basheer M. Al-Maswari [a,b,*], Eman Ramadan Elsharkawy [c,*], Awatif Rashed Z. Almotairy [d], Khaled Alkanad [e], Abdelkader Zarrouk [f], Fatima A.S. Al-Yusufy [g], B.M. Venkatesha [b,*]

[a] Department of Chemistry, Faculty of Applied Sciences and Humanities, Amran University, Amran, Yemen
[b] Department of Chemistry, Yuvaraja's College, University of Mysore, Mysuru 570005, Karnataka, India
[c] Center for Health Research, Northern Border University, Arar73213, Saudi Arabia
[d] Department of Chemistry, College of Science, Taibah University, Yanbu Governorate, Saudi Arabia
[e] Department of Studies in Physics, University of Mysore, Manasagangotri, Mysuru 570006, India
[f] Laboratory of Molecular Spectroscopy Modelling, Materials, Nanomaterials, Water and Environment, CERNE2D, Faculty of Sciences, Mohammed V University in Rabat, Morocco
[g] Department of Chemistry, College of Science, Qassim University, Ar Rass 51921, Saudi Arabia

ARTICLE INFO

Keywords:
N-doped carbon QDs
Novel electrode
Barium ferrite
Magnetic nanocomposite
Energy storage
Supercapacitors

ABSTRACT

Nitrogen-doped carbon quantum dots (NCQDs) have garnered considerable interest in energy storage applications owing to their remarkable electrical characteristics and surface adaptability. In this regard, barium ferrite (BFO) nanocomposites with NCQDs have been incorporated due to their remarkable electrochemical performance in supercapacitors. Where NCQDs with an average particle size of about 3 nm were prepared using a simple hydrothermal approach and then combined with barium ferrite (BFO) to create a novel magnetic nanocomposite (BFO@NCQDs). The NCQDs functioned as structure-directing agents, facilitating exact regulation of the size, crystallinity, and shape of the BFO nanoparticles. The structural and morphological characteristics of the synthesized nanocomposite were thoroughly characterized using PXRD, Raman spectroscopy, FTIR, FE-SEM, and HRTEM. Magnetic studies revealed a saturation magnetisation (*Ms*) of 50.59 emu/g and a notably increased specific surface area (SA_{BET}) of 821.65 m^2/g. Electrochemical assessments in a 5 M KOH electrolyte using a three-electrode configuration demonstrated exceptional performance, attaining a specific capacitance (*Cs*) of 1513.94 F/g at a scan rate of 5 mV/s, by ascertained using cyclic voltammetry. Galvanostatic charge/discharge analysis confirmed a high specific capacitance of 1984.98 F/g at a current density of 2 A/g. The electrode exhibited remarkable energy and power densities, achieving 42.805 Wh/kg and 7565.43 W/kg, respectively, while sustaining a power density of 2090.39 W/kg at peak energy output. The electrode material exhibited exceptional cycling stability, maintaining 91.1 % of its capacitance after 10,000 cycles at 12 A/g. The findings underscore BFO@NCQDs as an economical, highly conductive, and resilient electrode material, positioning it as a viable option for next-generation supercapacitors and portable electronic applications.

1. Introduction

The global transition toward renewable and sustainable energy systems has intensified the need for efficient energy storage technologies. Among these, supercapacitors (SCs) have emerged as a promising solution due to their high power density, rapid charge–discharge rate, long cycle life, and economic feasibility [1–3]. Despite these advantages, SCs remain limited by their relatively low energy density, which significantly constrains their practical applications. The properties and nature of electrode materials are pivotal in influencing the electrochemical efficacy of SCs [4], necessitating the innovation of excellent-performance electrodes to attain SCs devices with elevated energy

* Corresponding authors at: Department of Chemistry, Yuvaraja's College, University of Mysore, Mysuru 570005, Karnataka, India.
E-mail addresses: basheer.almaswari@gmail.com (B.M. Al-Maswari), elsharqawyeman2017@gmail.com (E.R. Elsharkawy), bmvenkatesha123@gmail.com (B.M. Venkatesha).

https://doi.org/10.1016/j.inoche.2025.115790
Received 27 August 2025; Received in revised form 4 October 2025; Accepted 3 November 2025
Available online 6 November 2025
1387-7003/© 2025 Elsevier B.V. All rights are reserved, including those for text and data mining, AI training, and similar technologies.

density. Supercapacitors are generally categorized into electric double-layer capacitors (EDLCs), pseudocapacitors, and hybrid supercapacitors (HICs) [5–8]. EDLCs typically employ porous carbon materials and store energy through electrostatic ion adsorption at the electrode/electrolyte interface. Although such materials offer excellent cycling stability, their capacitance is largely confined to surface area effects, limiting overall energy density [9–11]. To overcome this, integrating materials with both high surface area and faradaic activity is essential, enabling rapid charge transfer and efficient redox reactions [12].

Carbon quantum dots (CQDs), a subclass of carbon nanomaterials with dimensions below 10 nm, have recently attracted attention as electrode modifiers due to their remarkable physicochemical features. These include quantum confinement effects, tunable bandgap, excellent electron transport properties, and abundant surface functional groups such as hydroxyl, carboxyl, and aldehyde [13–16]. CQDs also offer stability, dispersibility, biocompatibility, and ease of synthesis, making them suitable for diverse applications in energy storage, catalysis, water treatment, and biomedicine [17–29]. Structurally, doping CQDs with heteroatoms (e.g., nitrogen) has been shown to enhance electronic characteristics and tune intrinsic properties, such as electronic and optical traits [30]. Nitrogen doping, in particular, introduces electron-rich active sites and enhances conductivity and redox kinetics, yielding nitrogen-doped CQDs (NCQDs) with superior electrochemical properties compared to undoped counterparts [31]. These features position NCQDs as highly promising for improving the performance of supercapacitor electrodes [12].

Parallel to carbon nanomaterials, ferrite-based compounds have gained attention for electrochemical energy storage due to their abundance, low-cost synthesis, and tunable electrical and magnetic properties [32,33]. They can be prepared from inexpensive precursors under moderate conditions [34], and exist in diverse structural families, including spinel, garnet, and magneto-plumbite ferrites [35]. Among them, spinel ferrites have been widely investigated for applications in catalysis, memory devices, antimicrobial nanocomposites, and electromagnetic absorbers owing to their chemical stability and magnetic versatility [36]. Among ferrites, barium ferrite ($BaFe_2O_4$, BFO) stands out as a magneto-plumbite structure with unique electrical and magnetic properties, multiple redox-active sites, and structural robustness. These characteristics make BFO a potentially valuable but underutilized candidate for supercapacitor electrodes. Despite progress in both carbon nanomaterials and ferrites, there remains a lack of systematic studies combining NCQDs with ferrite compounds, particularly BFO.

To fill this gap, the present study reports the development of a novel electrode incorporating N-doped carbon quantum dots (NCQDs) mixed with barium ferrite $BaFe_2O_4$ (BFO) to create a magnetic nanocomposite (BFO@NCQDs) for supercapacitor applications in energy storage. The design enhances the synergistic interaction between the electron-donating/withdrawing functionalities of nitrogen dopants and the redox-active, magnetic properties of ferrite. The BFO@NCQDs magnetic nanocomposite exhibited excellent electrochemical properties due to its porous nature and large surface area, which provided numerous active sites for redox mechanisms. Overall, this work introduces BFO@NCQDs as a new class of electrode material for high-performance supercapacitors. By combining the unique advantages of NCQDs and ferrites, the nanocomposite demonstrates enhanced energy density and cycling stability, contributing to the advancement of sustainable energy storage technologies.

2. Materials and methodology

2.1. Precursors

The utilized chemicals acquired from Sigma Aldrich; Iron (III) nitrate nonahydrate ($Fe(NO_3)_3{\cdot}9H_2O$) purity 99.999 %, Barium nitrate Ba $(NO_3)_2.4H_2O$ (99.999 %), Citric acid ($C_6H_8O_7.H_2O$) 99.9 %, urea (purity 99 %), Melamine ($C_3H_6N_6$), and Sucrose ($C_{12}H_{22}O_{11}$) were used to obtain the precipitate. Distilled water, acetone, and ethanol were used to wash off the sediment.

2.2. Synthesis of BFO@NCQDs magnetic nanocomposite

The synthesis of the BFO@NCQDs magnetic nanocomposite electrode for supercapacitor applications was carried out in three steps (Scheme 1). *In the first step*, N-doped carbon quantum dots (NCQDs) were produced utilizing melamine and sucrose as nitrogen and carbon sources, respectively. Precisely, 0.126 g (16 wt%) of melamine was solubilized in 60 mL of nano pure water and agitated continuously at 70 °C for 60 min. Subsequently, 1.7 g (0.005 mol) of sucrose was incorporated into the resulting translucent solution, and the combination was stirred at 70 °C for a further 60 min to get a mixture designated as (MS). The resultant solution was thereafter transferred into an autoclave reactor lined with Teflon at 180 °C for a duration of 5 h. The resultant product was subjected to two washes with ethanol/H_2O and subsequently dehydrated under vacuum at 50 °C for 12 h, yielding NCQDs in the form of a fine powder. *In the second step,* which that simultaneously with step one, sol-gel nanoparticles of $BaFe_2O_4$ were produced. In this process, 8.08 g (0.02 mol) of $Fe(NO_3)_3.9H_2O$ and 3.3334 g (0.01 mol) of Ba $(NO_3)_2.4H_2O$ were liquified in 50 mL of a 1 M urea solution (prepared with distilled water) under magnetic stirring at 70 °C. Subsequently, 10.5072 g (0.046 mol) of $C_6H_8O_7.H_2O$ was then added to the mixture, maintaining a 1:1 M ratio of metal ions to $C_6H_8O_7.H_2O$ to facilitate the formation of nanospheres (referred to as $BaFe_2$-UC). After 60 min of stirring at 70 °C, the mixture had formed a gel, which needed another 4 h of stirring to reach the required viscosity. The organic residues were removed from the gel by calcining it at 850 °C for 8 h, resulting in $BaFe_2O_4$ (BFO) nanoparticles. *In the third and final step,* the BFO@NCQDs nanocomposite was prepared by mixing 100 mg of $BaFe_2O_4$ (BFO) and 100 mg of NCQDs in 200 mL of deionized water, stirring for 30 min, and thereafter subjecting it to ultrasonic treatment for 15 min. The resultant mixture was placed in an autoclave lined with Teflon, sealed, and subjected to heating at 180 °C for 8 h. The final product, BFO@NCQDs nanocomposite, underwent extensive washing with nano pure water, acetone, hot water, and ethanol. After that, it was dried for 24 h at 60 °C.

2.3. The electrochemical (EC) experiments

The EC characteristics of the BFO@NCQDs electrode were measured utilizing a 3-electrode system with a CHI 608e electrochemical workstation, as previously cited in literature [10,37,38]. We conducted electrochemical investigations utilizing electrochemical impedance spectroscopy (EIS), Cyclic voltammetry (CV), and Galvanic charge/discharge (GCD). The specific capacitance (*Cs*) values of the BFO@NCQDs electrode were calculated at various scan rate (S_R) and current density (I_d) using eqs. (1 and 2) [5].

$$C_s = \frac{\int I(V)dV}{m \times \Delta V \times \nu} \quad F \Big/ g \tag{1}$$

$$C_s = \frac{I \times \Delta t}{m \times \Delta V} \quad F \Big/ g \tag{2}$$

3. Results and discussions

3.1. XPS analysis

The structure of BFO@NCQDs was further clarified through XPS analysis. Fig. 3.1(a) illustrates the survey spectrum of the $BaFe_2O_4$@NCQDs magnetic nanocomposite, showing characteristic peaks for Ba, C, N, O, and Fe elements within the (0–900 eV) range. These peaks confirm the high phase purity of the BFO@NCQDs composite, with the peak attributed to adventitious carbon from the XPS

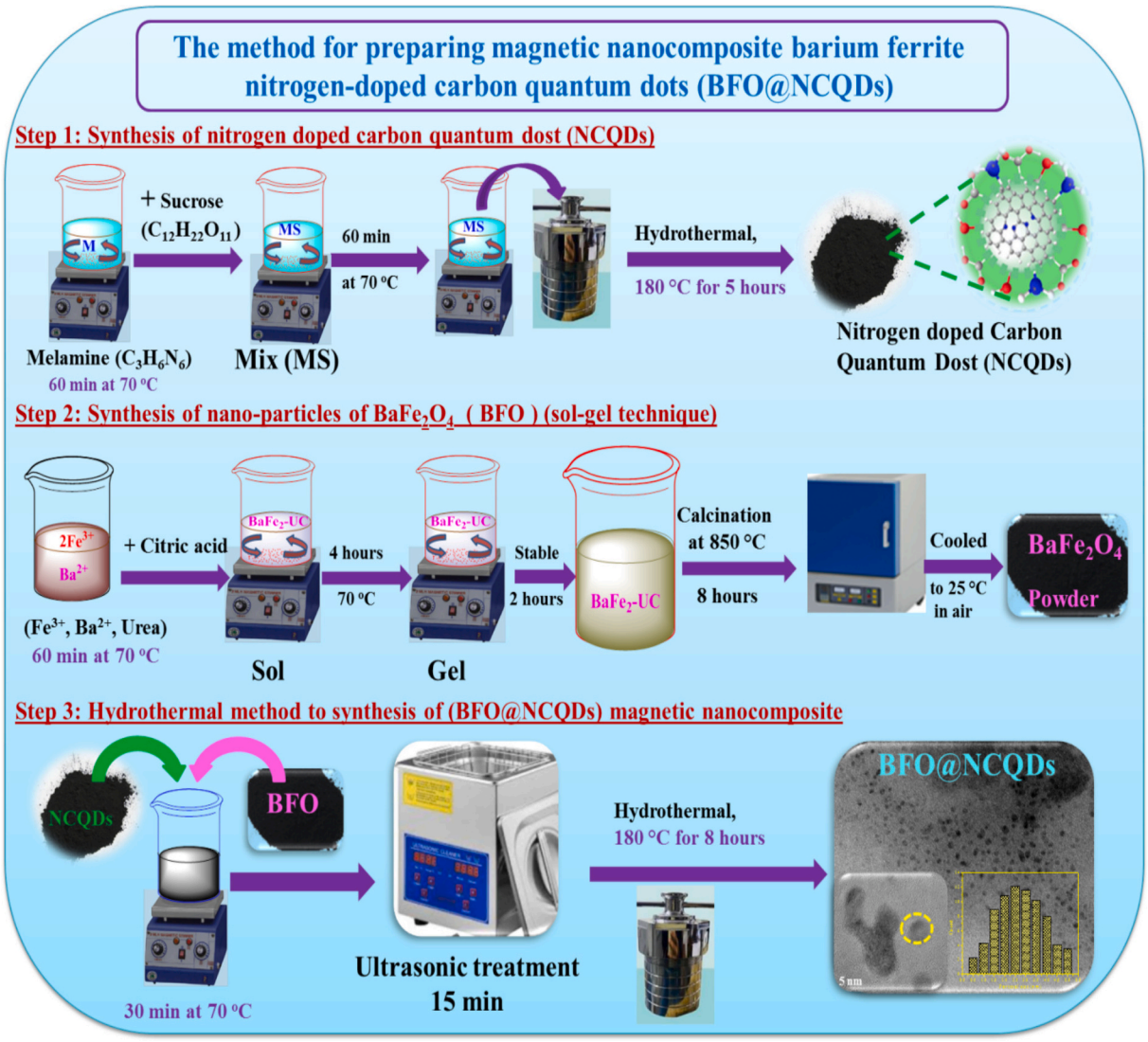

Scheme 1. The method for preparing nitrogen-doped carbon quantum dots combined with magnetic nanocomposite barium ferrite (BFO@NCQDs)

spectrum, further confirming the composite's purity [39]. The Ba 3d spectra shown in Fig. 3.1(b) have binding energies of 780.8 eV for Ba $3d_{5/2}$ and 796.1 eV for Ba $3d_{3/2}$, according to references [39, 40]. The Fe 2p spectra is displayed in Fig. 3.1(c), Fe $2p_{3/2}$ and Fe $2p_{1/2}$ peaks at 710.9 eV and 724 eV, respectively, closely aligning with existing literature [39–41]. There were three satellite peaks at: 719.26, 731.57, and 734.53 eV. These findings point to the presence of Fe^{3+} cations in the materials that were produced. Three peaks are discernible in the high-resolution (HR) O 1 s spectra shown in Fig. 3.1(d): the lattice oxygen (C—O) in the BFO@NCQDs magnetic nanocomposite at 532.72 eV, the surface -O-H of water molecules at 531.28 eV, and a Ba/Fe-O bond at 530.28 eV [5,40,41]. Graphitic, pyrrolic, and Pyridinic-N are represented by the three deconvoluted peaks in the N 1 s spectra in Fig. 3.1(e) at 400.27, 399.6, and 398.80 eV, respectively [5,10,42]. The combination of different nitrogen configurations can lead to synergistic effects that further enhance electrochemical performance. Nitrogen-doped carbon materials exhibit high specific capacitance and excellent cycling stability, attributed to the presence of various nitrogen functionalities that provide active sites and improve conductivity [38,43]. There are four deconvoluted peaks at 284.67, 286.04, 287.13, and 288.11 eV in the HR-XPS spectra of C 1 s shown in Fig. 3.1(f). These peaks are attributed to C-C/C=C, C═N, C—N, and C═O, respectively [5,40,41,44]. According to the XPS results, the BFO@NCQDs magnetic nanocomposite does indeed contain N-doped graphite carbon [40].

3.2. XRD analysis

The phase purity of the BFO@NCQDs magnetic nanocomposite was evaluated by powder X-ray diffraction (PXRD), as illustrated in Fig. 3.2. According to the referencing JCPDS 00–025-1191, the XRD results validate the crystalline structure of BFO@NCQDs with a cubic spinel structure of barium monoferrite $BaFe_2O_4$. The peaks observed at (210), (111), (402), (212), (610), (020), (004), (802), (422), (214), (614), (822), and (630) with corresponding 2θ positions of 18.8°, 20.0°, 28.1°, 28.4°, 32.7°, 33.2°, 42.6°, 43.5°, 44.1°, 54.8°, 56.5°, 58.0°, and 59.0°, respectively [45]. The XRD analysis also reveals the presence of NC in the BFO@NCQDs, through the appearance of the peaks at (002), (100), and (004) corresponding to 2θ of 25.17°, 43.73°, and 55.18°, respectively [10,41,46], suggesting that the synthesized graphene is not in a pure monolayer form. These findings are further supported by electron microscopy studies, which align with the XRD results.

3.3. FTIR spectra analysis

The BFO@NCQDs' FTIR spectra in the 400–4000 cm^{-1} region are shown in Fig. 3.3. O-H/N-H, C—H, C—C, C═O, C═N, and C—N

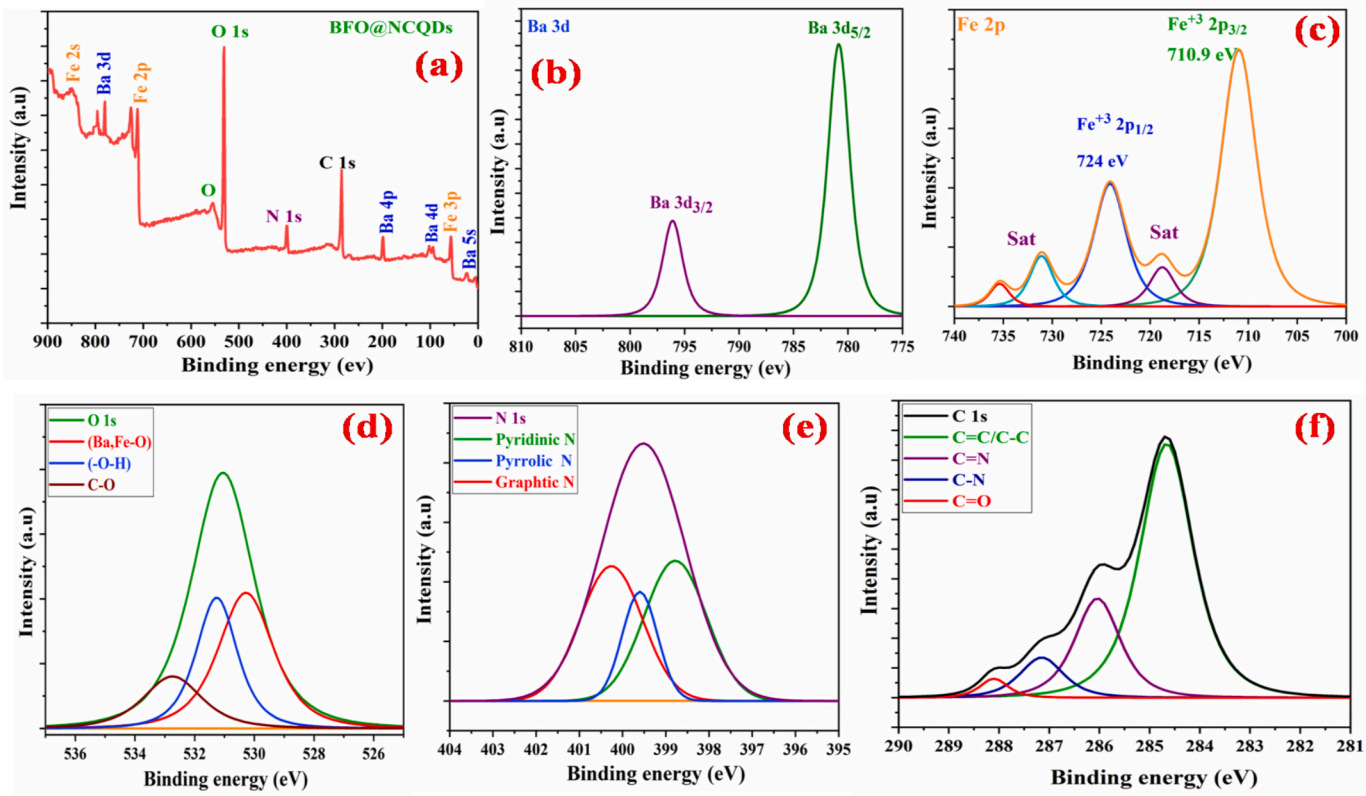

Fig. 3.1. (a) XPS survy spectra of BFO@NCQDs, HR-XPS for (b) Ba 3d, (c) Fe2p, (d) O1s, (e) N1s, and (f) C1s.

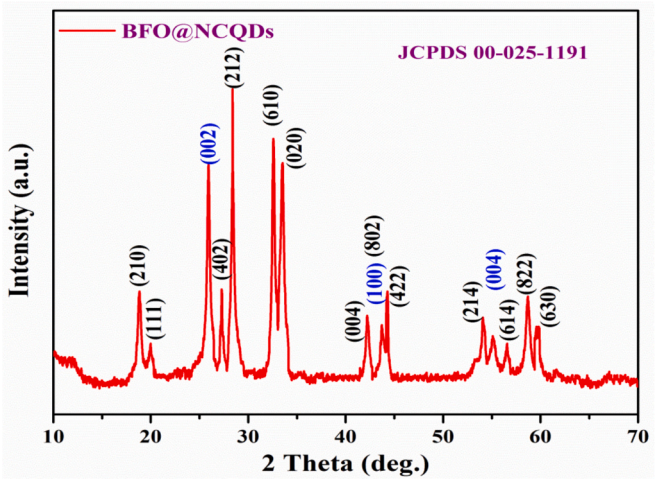

Fig. 3.2. Powder X-ray diffraction (PXRD) analysis of BFO@NCQDs magnetic nanocomposite.

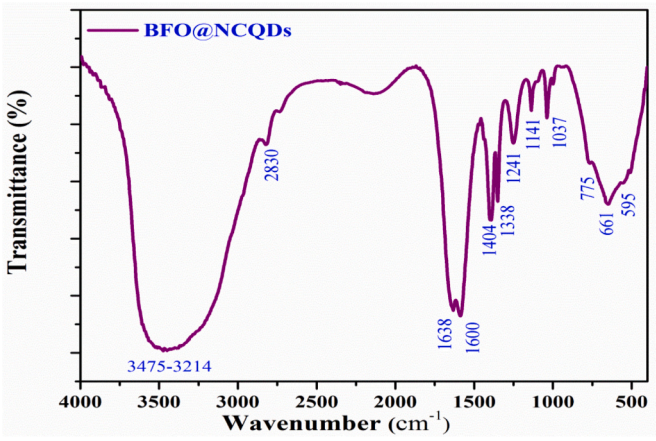

Fig. 3.3. Fourier transform infrared spectrometer (FTIR) of BFO@NCQDs magnetic nanocomposite.

functional groups are responsible for the strong stretching vibration bands found in the spectra at 3475–3214, 2830, 1638, 1600, 1404, and 1241 cm^{-1}, correspondingly [41,47,48]. The aromatic C—N heterocyclic modes, which exhibit the stretch and rotate vibrations of C═N and C—N bonds, are represented by vibrational bands between 1241 and 1638 cm^{-1} [49,50]. The graphite carbon's nitrogen sources are broken down by organic substances such as sucrose, urea, melamine, and citric acid [41,47]. The band at 1338 cm^{-1} is accredited to N—H bending, whereas the vibrational stretch of aromatic C—O and C—N, coupled with C—H bending, corroborates the existence of nitrogen in the composites in pyrrolic and pyridine forms, further validated by XPS analysis [5,41,51]. The bands at 1141 and 1037 cm^{-1} signify C—O stretching from epoxy and alkoxide groups, respectively [52,53]. Bands at 661 and 775 cm^{-1} are accredited to Ba—O stretching in tetrahedral sites [54]. A strong absorption band at 595 cm^{-1} represents Fe—O stretching, characteristic of $BaFe_2O_4$ nanocrystals. The peaks at 595, 661, and 775 cm^{-1} designate vibrations due to metal ions Fe^{3+}, Ba^{2+}/O^{2-} in octahedral and tetrahedral configurations, with high-frequency bands corresponding to metal oxide bonds at tetrahedral sites and low-frequency bands at octahedral sites, characteristic of spinel ferrites [45,55].

3.4. N_2 adsorption-desorption isotherm(BET) analysis

The porous structure of the BFO@NCQDs magnetic nanocomposite was confirmed using the N_2 adsorption-desorption isotherm, as illustrated in Fig. 3.4. A type IV isotherm was observed for the BFO@NCQDs,

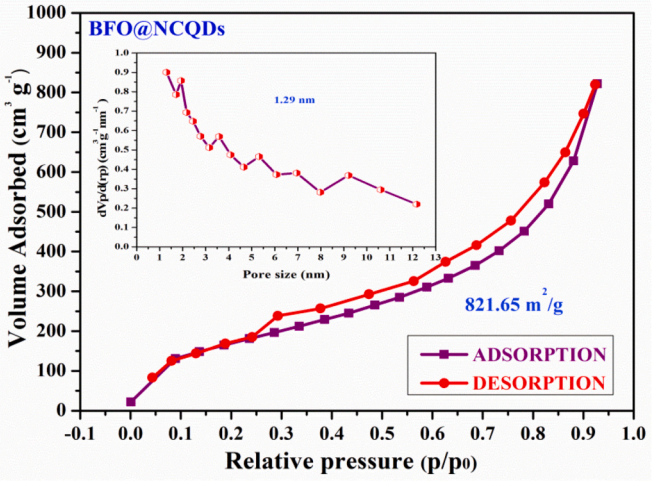

Fig. 3.4. N_2 adsorption-desorption isotherm (BET) of BFO@NCQDs magnetic nanocomposite.

signifying a mesoporous structure with a surface area (SA_{BET}) of 821.65 m^2/g. As seen in the inset of Fig. 3.4, the BJH model measures the pore size distribution, which averages 1.29 nm. The mesoporous structure allows for efficient transport of electrolyte ions, and a high SA_{BET} indicates a large surface area of active sites [56,57].

3.5. Raman spectroscopy analysis

The structure of the BFO@NCQDs magnetic nanocomposite and the production of graphitic carbon were studied using Raman spectroscopy. The graphitic (G) band and the defect (D) band are distinguished by two conspicuous peaks in Fig. 3.5 at 1580.43 and 1344.87 cm^{-1}, respectively. The doubly degenerate E_{2g} phonon is the source of the G-band, whereas the E_{2g} mode of sp^2-ring graphitic carbon is linked to the D-band [58,59]. The I_D/I_G ratio of 1.07 signifies a high-quality grade of graphite characterized by intrinsic voids and pores within the carbon framework, which augment the surface area and active sites. Furthermore, the BFO@NCQDs magnetic nanocomposite displayed supplementary low-intensity peaks at 695, 504.9, 317.6, and 211.27 cm^{-1}. These peaks correspond to the symmetric and asymmetric stretching of oxygen atoms bonded to metals (Ba and Fe) in tetrahedral and octahedral coordination. They confirm the typical normal spinel structure of $BaFe_2O_4$ in the BFO@NCQDs magnetic nanocomposite [41,53].

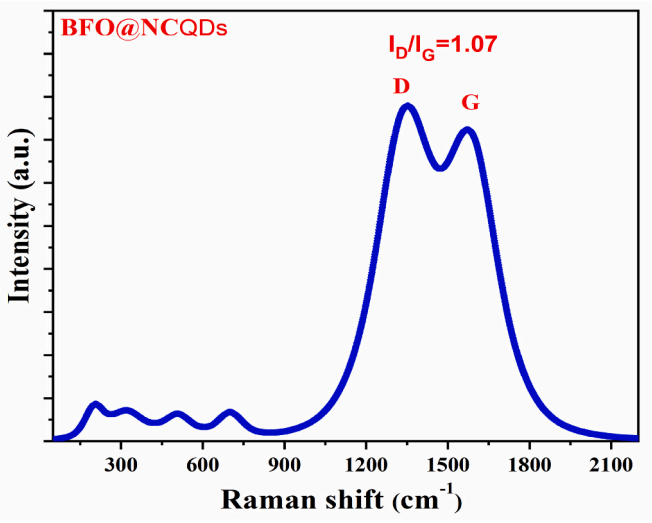

Fig. 3.5. Raman spectrum of BFO@NCQDs magnetic nanocomposite.

3.6. Vibrating-sample magnetometry (VSM) analysis

The ability to combine high electrical capacitance with advanced ferrimagnetic or ferromagnetic properties in a single material at room temperature opens an avenue for the development of advanced magnetically ordered capacitive materials. Recent studies highlight the excellent capacitive performance of ferrite-based compounds, which combine room-temperature ferromagnetism and giant negative magnetoresistance. The coupling of high capacitance and magnetization in magnetically ordered capacitive materials provides a platform for strong magnetoelectric interactions. Magnetocapacitance studies show a significant increase in the capacitance of magnetically ordered capacitive materials under the influence of a magnetic field. The field also enhances energy and power density, reduces resistance, and improves cycling stability [60]. Ferromagnetic materials are materials that are strongly attracted to an external magnetic field. This type of material has more unpaired electrons in its metal atoms or metal ions. Thus, any excitation of the ferromagnetic material causes a transfer of individual electrons. This transfer increases the electrical conductivity (electrochemical), greatly benefiting supercapacitors and energy storage devices [61]. Recently, magnetic field-induced electrochemical energy storage performance has opened up new possibilities for supercapacitor research. The noncontact energy provided by the magnetic field can affect the electrochemical performance of a supercapacitor by inducing changes in the electrode and electrolyte at the molecular level. The magnetic field can rearrange the electronic and ionic distribution and accelerate ionic transport at the electrode/electrolyte interface. The magnetic field can also induce structural and morphological changes during electrode fabrication, which has a significant impact on their electrochemical activity [62]. Fig. 3.6 illustrates the magnetic characteristics of the BFO@NCQDs, analyzed via vibrating-sample magnetometry (VSM) with an applied field of ±20 kOe at 25 °C. The results revealed that the coercivity (*Hc*), saturation magnetization (*Ms*), remanent magnetization (*Mr*), and the *Mr/Ms* ratio were 809.39 Oe, 50.59 emu/g, 26.31 emu/g, and 0.520, respectively [63,64].

3.7. TGA-DTA analysis

To assess the thermal characteristics of the BFO@NCQDs precursor and optimize its calcination conditions, TGA-DTA analysis was performed up to 900 °C, as displayed in Fig. 3.7. The evaporation of adsorbed moisture was responsible for an initial weight loss of 13.45 %

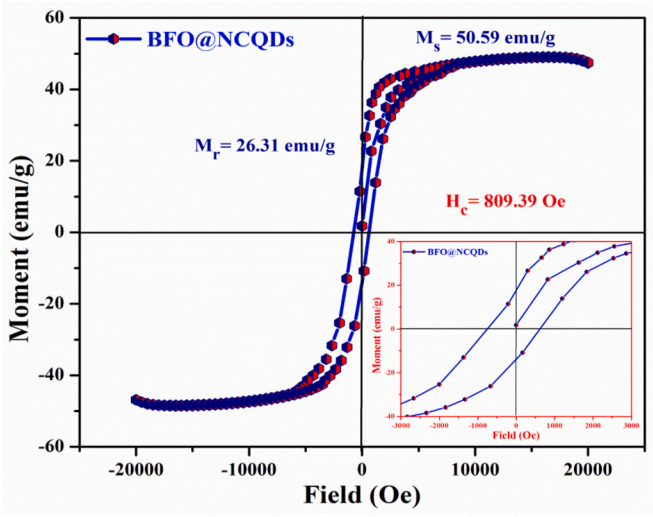

Fig. 3.6. Vibrating-sample magnetometry (VSM) curve of BFO@NCQDs magnetic nanocomposite that displays saturation magnetization and remanent magnetization values.

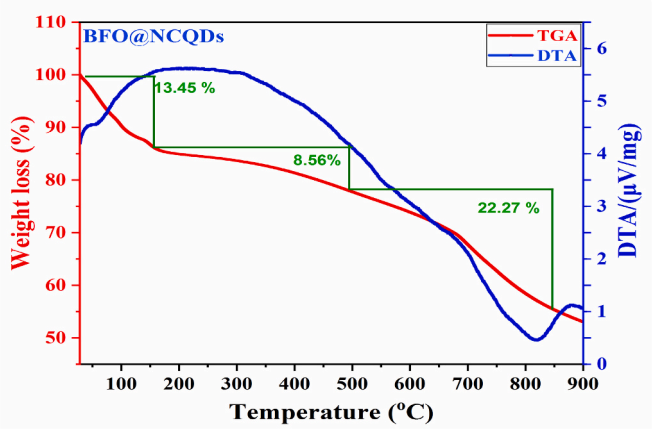

Fig. 3.7. TGA/DTA analysis that displays the thermal characteristics of BFO@NCQDs magnetic nanocomposite.

in the range of 25–150 °C. In the second phase, occurring between 150 and 500 °C, and in the third phase, occurring between 500 and 700 °C, additional weight losses of 8.56 % and 22.27 %, respectively, were noted as a result of the thermal degradation of organic compounds [5,41,65]. The DTA curve of $BaFe_2O_4$ is an essential instrument for assessing the thermal properties of this material and comprehending its synthesis and phase change mechanisms. The DTA curve of $BaFe_2O_4$ will exhibit exothermic peaks indicative of different thermal phenomena, including phase changes and crystallization. The peaks can be utilized to ascertain the synthesis temperature and the precise temperature intervals at which certain phases develop. Exothermic peaks, with the first peak at 196 °C as a phase transition [65], and the second peak at around 860 °C, are frequently linked to the crystallization of barium monoferrite during pyrosynthesis, resulting in the creation of $BaFe_2O_4$ from its precursor components [66].

3.8. TEM analysis

The geometric structure of the pristine NCQDs and BFO@NCQDs was analyzed using TEM imaging. Fig. 3.8 illustrates the unique characteristics of the original components and provides details about the overall architecture of the heterostructure. Fig. 3.8(a) presents the TEM image of pristine NCQDs, revealing a distribution of spherical shape with a size ranging from 0.5 to 5 nm. This observation indicates that the hydrothermal treatment effectively fragmented nanometer-sized graphene sheets into smaller quantum dots. The size and crystal structure of the produced NCQDs were further validated through HR-TEM imaging. From Fig. 3.8(b), the lattice spacing of the NCQDs is found to be 0.343 nm, which matches the (002) plane of graphitized carbon. For the BFO@NCQDs heterostructure, the TEM image Fig. 3.8(c) reveals a homogeneous distribution of spherical NCQDs interspersed with clusters of BFO nanoparticles within a layered carbon matrix. This integration significantly reduces the crystallinity of the NCQDs by increasing the quantity of binding and conducting agents. This phenomenon is attributed to electrostatic interactions, dipole-dipole interactions, and hydrogen bonding involving surface functional groups during the hydrothermal treatment. These interactions facilitate the creation of graphene carbon QDs and their subsequent interaction with Ba (II) and Fe (III) cations, as well as urea [67]. This mechanism influences crystal growth, thus altering the morphology of the final material. HR-TEM analysis (Fig. 3.8d and e) confirms that the BFO nanoparticles effectively encapsulate the NCQDs, creating close interfacial contact between the phases in the heterostructure. The lattice spacing of 0.343 nm in the NCQDs matches the (002) plane of graphene carbon, whereas the lattice spacings of 0.327 nm and 0.273 nm, associated with $BaFe_2O_4$, align with the (212) and (610) planes of $BaFe_2O_4$, respectively. Results from XRD corroborate these findings, which point to robust chemical associations

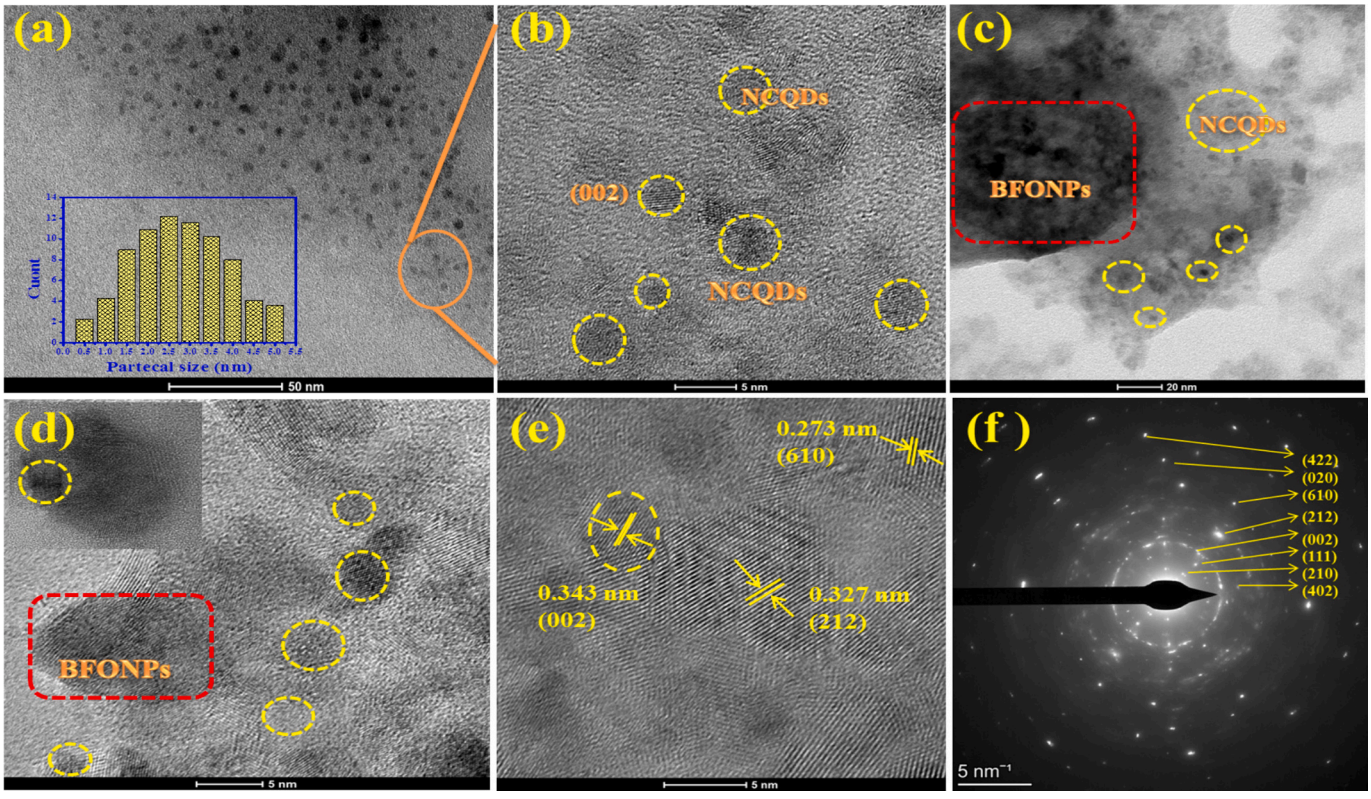

Fig. 3.8. Morphological analysis of synthesized sample (a) TEM images and size distributions, (b) HR-TEM images of pure NCQDs, (c) TEM images, (d,e) HR-TEM images, and (f) SAED of BFO@NCQDs magnetic nanocomposite.

between BFO nanoparticles and oxygen-containing functional groups on NCQDs, as well as van der Waals interactions between BFO and NCQDs [5,35,45,64,67]. The selected area electron diffraction (SAED) of BFO@NCQDs is displayed in Fig. 3.8(f). The shown patterns exhibit seven intense rings, corresponding to the (210), (111), (402), (212), (610), (020), and (422) planes of $BaFe_2O_4$. An additional ring indexed to the (002) plane further confirms the presence of graphitic carbon. Together, these results provide clear evidence of the structural and chemical integration within the BFO@NCQDs magnetic nanocomposite.

To confirm the high crystallinity of the prepared BFO@NCQDs magnetic nanocomposite and the homogeneous distribution of spherical NCQDs on the BFO nanosheets, elemental mapping analysis was performed, as shown in Fig. 3.9. The extremely demonstrate distribution of the elements (Ba, O, N, Fe, and C) within the nanosheets is clearly shown by the elemental mapping images of the BFO@NCQDs. This signifies the similar distribution of NCQDs on the surface of the BFO nanosheets within the BFO@NCQDs magnetic nanocomposites.

4. Electrochemical performance studies of the BFO@NCQDs electrode

4.1. Cyclic voltammetry analysis (CV)

The electrochemical efficacy of the BFO@NCQDs magnetic heterostructure as an excellent electrode for SCs was assessed at ambient temperature. CV measurements were conducted at various scan rates (S_R) ranging from 5 to 50 mV/s using a 5 M KOH solution as the electrolyte, within a potential between (−0.3 to +0.4 V), as illustrated in Fig. 4.1(a). The maximum *Cs* of the BFO@NCQDs electrode was calculated to be around 1513.94 F/g at a scan rate (S_R) of 5 mV/s, as illustrated in Fig. 4.1(b) using Eq. (1). The electrochemical reaction seen in the CV analysis, as illustrated by Eqs. (3–9), lends credence to the EDLC behavior. This efficiency is due to the fact that the physical and porosity properties of the material facilitate contact between the electrode surface and the electrolyte ions.

$$BaO + Fe_2O_3 \leftrightarrow BaFe_2O_4 \quad (3)$$

$$Fe^{3+} + 3OH^- \rightarrow Fe(OH)_3 \quad (4)$$

$$3Fe(OH)_3 + 3e^- \rightarrow 2FeO_2^- + 4H_2O + OH^- + Fe^{(0)} \quad (5)$$

$$2Fe^{(0)} + 6OH^- \leftrightarrow Fe_2O_3 + 3H_2O + 6e^- \quad (6)$$

$$Ba^{2+} + 2OH^- \rightarrow Ba(OH)_2 \quad (7)$$

$$2\,Ba(OH)_2 + 2e^- \rightarrow BaO + H_2O + 2OH^- + Ba^{(0)} \quad (8)$$

$$Ba^{(0)} + 2OH^- \leftrightarrow BaO + H_2O + 2e^- \quad (9)$$

4.2. Galvanic charge/discharge analysis (GCD)

In the same vein, GCD experiments were carried out with a voltage ranging between 0.0 and 1.4 V and varying current density (I_d) values from 2 to 12 A/g, as displayed in Fig. 4.2(a). By utilizing the GCD rates of the BFO@NCQDs magnetic nanocomposites at various discharge currents (I_d) [5], the *Cs* of the electrode in a three-electrode system was determined using Eq. (2). At I_d of 2, 4, 6, 8, 10, and 12 A/g, the specific capacitance values that resulted were 1984.98, 1614.65, 1413.96, 1252.8, 1126.38, and 938.4 F/g, respectively, as shown in Fig. 4.2(b).

4.3. The symmetric cell of the BFO@NCQDs electrode analysis

A Ragone plot illustrating the BFO@NCQDs magnetic nanocomposite's overall performance is shown in Fig. 4.3. Eqs. (10−12) were used in a two-electrode system to determine the specific capacitance C_t (F/g), energy density (E_t) (Wh/kg), and power density(P_t) (W/kg) of the symmetric electrode.

$$C_t = \frac{4I \times \Delta t}{m \times \Delta V} \qquad F/g \quad (10)$$

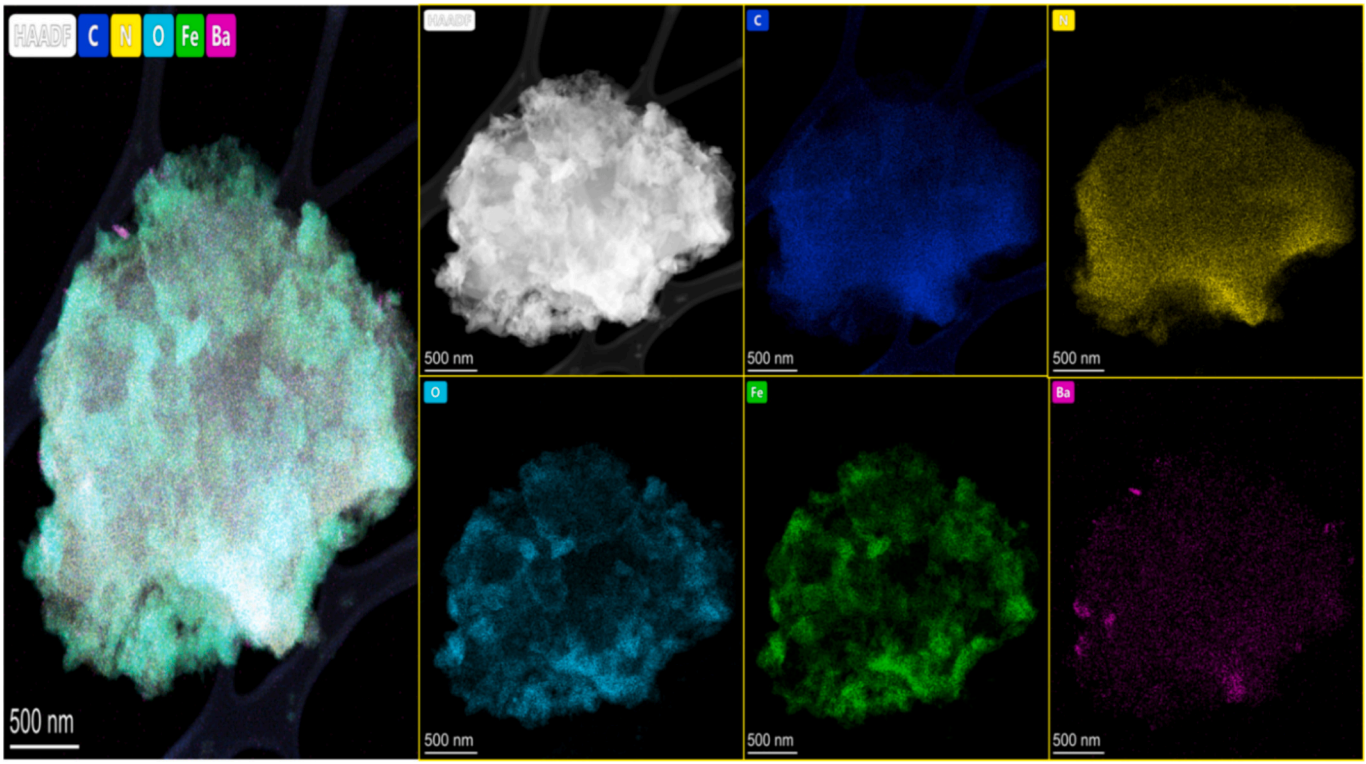

Fig. 3.9. Elemental mapping images of the BFO@NCQDs nanosheet, which illustrate the distribution of the elements in the sample.

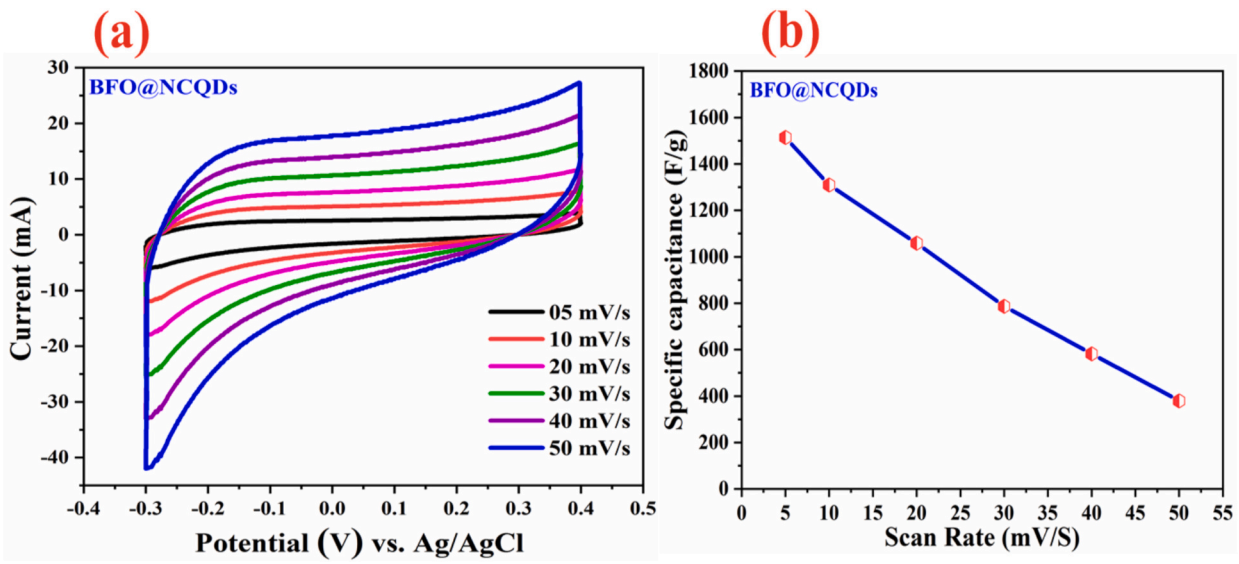

Fig. 4.1. Electrochemical analyses of BFO@NCQDs electrode (a) cyclic voltammetry (CV) at various scan rates ranging from 5 to 50 mV/s within a potential range between (−0.3 to +0.4 V), (b) specific capacitance (*Cs*) by CV.

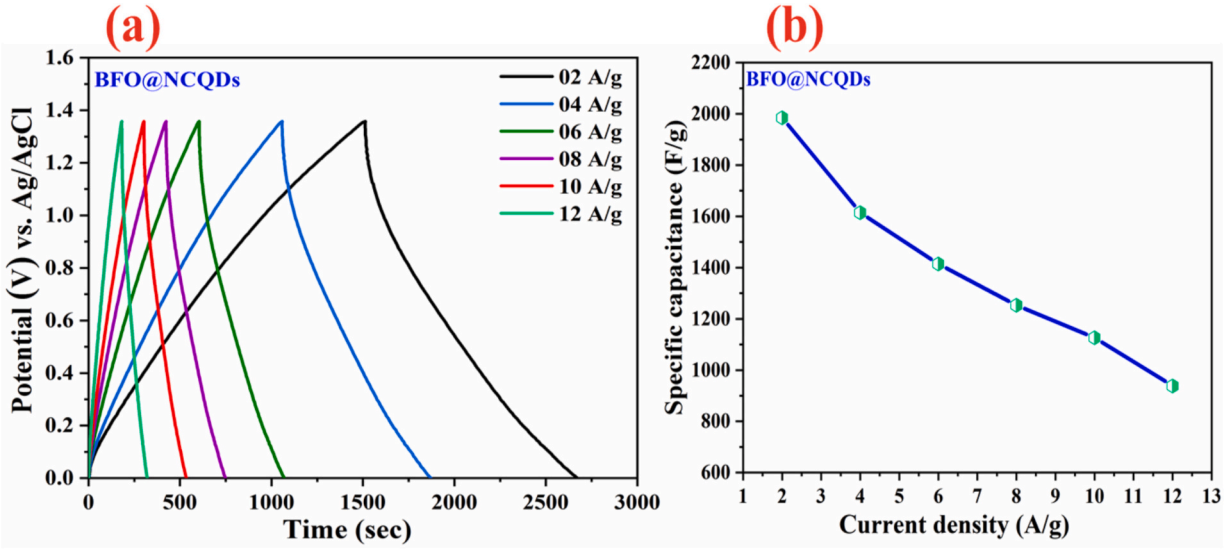

Fig. 4.2. Electrochemical analyses of BFO@NCQDs electrode (a) Galvanic charge/discharge (GCD) at current density values from 2 to 12 A/g, and (b) specific capacitance (*Cs*) by GCD.

$$E_t = \frac{1}{8 \times 3.6} C_t \Delta V 2 \qquad \text{Wh} \Big/ \text{kg} \tag{11}$$

$$P_t = \frac{E_t}{\Delta t} \times 3600 \qquad \text{W} \Big/ \text{kg} \tag{12}$$

The symmetric cell achieved (E_t) values of approximately 42.805, 31.326, 26.189, 22.065, 18.829, and 17.018 Wh/kg at corresponding (P_t) values of 2090.39, 2848.09, 3532.13, 4584.85, 5812.29, and 7565.43 W/kg. As seen in the inset of Fig. 4.3, the values of E_t decreased from 42.805 to 17.018 Wh/kg, P_t increased from 2090.39 to 7565.43 W/kg. This demonstrates that the BFO@NCQDs magnetic nanocomposite offers exceptional energy and power densities, critical for both environmental sustainability and commercial applications [68]. The symmetric electrode material of BFO@NCQDs exhibits improved performance for several reasons. Adding N-doped carbon QDs lowers the charge transfer resistance and increases the specific capacitance and electronic conductivity. Additionally, these quantum dots enhance interaction by making carbon compounds more wettable in the electrolyte. The BFO@NCQDs electrode has a lower internal resistance, which allows the active material and electrolyte to transfer charges more quickly. Furthermore, when a highly ion-conductive water electrolyte is present, the electrode's electric double-layer capacitance (EDLC) characteristics enable efficient charge transfer. Rapid and transitory faradic reactions are enabled by the high electroactive surface area (SA) of the BFO@NCQDs, which provides a short transportation route for electrolytes. Consequently, these nanomaterials demonstrate excellent potential for advanced energy storage applications [69–72].

4.4. The electrochemical impedance spectroscopy (EIS) analysis

Fig. 4.4 presents the EIS results of the BFO@NCQDs magnetic nanocomposites, depicted as a Nyquist plot. There is a semicircular area and a linear section on the plot. The electrolyte-electrode interface charge transfer resistance (R_{ct}) is represented by the semicircular region,

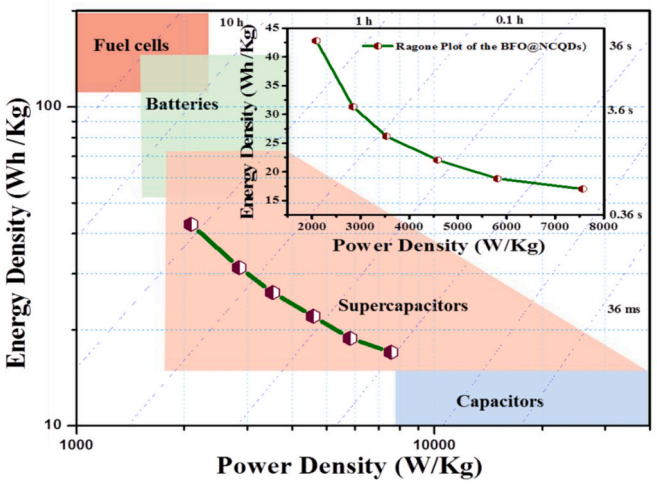

Fig. 4.3. Ragon plot of BFO@NCQDs magnetic nanocomposites, with an inset illustrating the changes in energy and power densities.

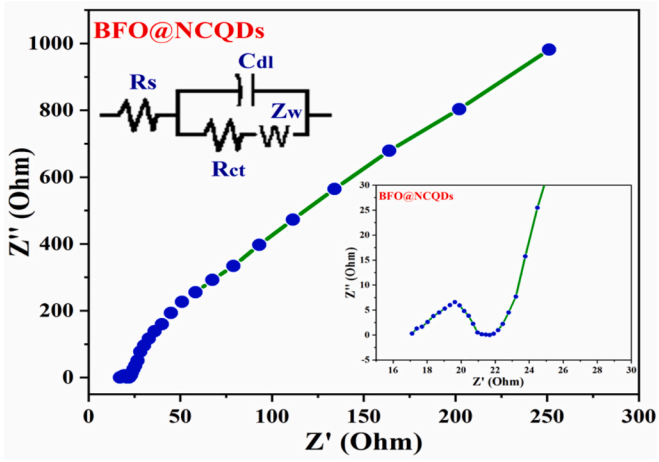

Fig. 4.4. The electrochemical impedance spectroscopy (EIS) curve of the BFO@NCQDs electrode, which contains the equivalent circuit model of the EIS spectrum.

and the ion diffusion within the electrode is reflected by the Warburg impedance (Z_w), which is represented by the linear section. The semicircle's diameter is used to calculate the interfacial resistance (R_{ct}), and the real axis intercept is used to estimate the internal resistance (R_s), which includes contact and electrolyte resistance [5,10]. Fig. 4.4 illustrates the equivalent circuit model for the EIS spectrum, which includes elements like Z_w, R_s, R_{ct}, and electric double-layer capacitance (C_{dl}). Approximately 17, 3, and 22 Ω were the observed values for R_s, R_{ct}, and Z_w in the BFO@NCQDs magnetic nanocomposites, which indicates great conductivity and stability [73–75]. Table 1 summarizes past research that compares the current work to that of other researchers and shows that the nitrogen-doped carbon QDs synthetic nanocomposite has better electrochemical performance as energy storage and supercapacitor electrodes.

4.5. Cyclic stability of BFO@NCQDs electrode analysis

At a discharge current of 12 A/g, the cyclic stability of the BFO@NCQDs electrode was evaluated using the GCD performance, as shown in Fig. 4.5. Because electrode materials are activated during cycling, the value of *Cs* gradually decreases [67,76,77]. As seen in the inset, which shows the electrode's performance after 10,000 cycles, it maintains 91.1 % of its initial *Cs*. This is illustrated by the last ten GCD cycles. The remarkable cyclic stability of BFO@NCQDs magnetic nanocomposites is attributed to their strong structure and morphology [77]. The electrode's Coulombic efficiency, which was already outstanding before 10,000 cycles at 12 A/g, stays at an even more astounding 99.9 %. The created BFO@NCQDs electrode's outstanding electrochemical performance is mainly attributable to the NCQDs, which have a high porosity and a large SA, as revealed in Fig. 3.4. These

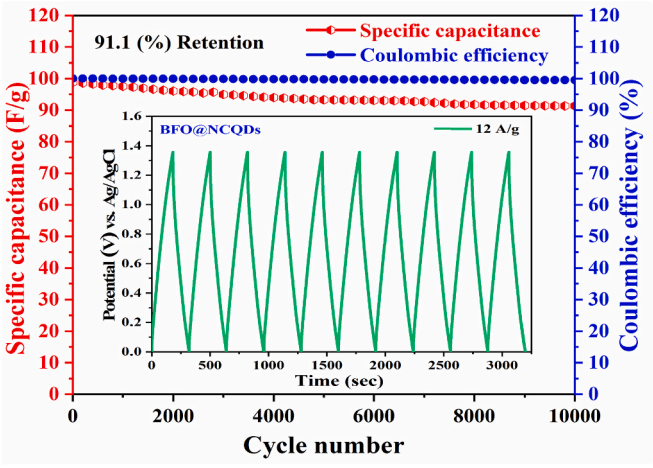

Fig. 4.5. Specific capacitance (*Cs*) and Coulombic efficiency against cycle number by the BFO@NCQDs electrode in the inset presents the last 10 GCD curves.

Table 1
Comparison of the present work with previously reported NCQDs as electrodes for supercapacitors and energy storage.

Material Electrode	Electrolyte	I_d (A/g)	E_t (Wh/Kg)	P_t (W/Kg)	*Cs* (F/g)	References
$BaFe_2O_4$@Cu_2O	$K_4[Fe(CN)_6]$	1	27	45	803	[78]
$BaFe_2O_4$	$K_4[Fe(CN)_6]$	1	–	–	593	[78]
$Ni(OH)_2$/NCDs	–	1	34.6	7000	1711.2	[79]
GQD/MnO_2	0.5 M Na_2SO_4	5 mV/s	0.154 μWh cm^{-2}	7.51 μW cm^{-2}	1170	[80]
Fe_2O_3QDs/FGS composites	1 M Na_2SO_4	0.1	50.7	100	347	[81]
$NiCo_2O_4$@ GQDs composite	6 M KOH	30	38	800	1242	[82]
$CuCo_2O_4$/ CQDs	PVA/KOH	1	39.5	1203.7	779.8	[83]
Fe_2O_3@CQDs	PVA/KOH	1	–	–	298.7	[83]
$NiCo_2O_4$ /C-QDs	–	1	27.8	10,240	856	[84]
(N-CQDs)/Co_3O_4 nanocomposite	6 M KOH	5 mV/s	36.9	480	1867	[85]
N-GQDs/Carbon Fiber /Graphene Hydrogel	–	20 mA/cm^3	20.5	200	93.7 F/cm^3	[86]
NCH/NCQDs	3 M KOH	1	49.1	–	727	[87]
BFO@NCQDs Magnetic Nanocomposite	5 M KOH	2	42.805	7565.43	1984.98	This work

properties prove that it is an ideal electrode for use in high-performance SCs, which store energy.

5. Scalability and cost considerations

The scalability and economic feasibility of electrode materials are critical for their practical use in energy storage devices. The BFO@NCQDs magnetic nanocomposite demonstrates clear advantages in this regard. Both barium ferrite and carbon quantum dots can be synthesized from abundant, inexpensive precursors, providing a sustainable alternative to expensive noble-metal-based systems. The hydrothermal method used for synthesis is simple, energy-efficient, and environmentally friendly, enabling large-scale production without the need for sophisticated equipment. Nitrogen doping, utilizing low-cost precursors such as urea or ammonia, further enhances electrochemical performance while maintaining minimal costs [38]. Recent studies also highlight that CQDs can be produced via green, low-cost, and scalable approaches, including electrochemical or biomass-derived carbonization [88,89]. Likewise, innovations in ferrite processing, such as two-step sintering, have significantly reduced energy consumption, reinforcing the scalability of ferrite-based nanomaterials [90]. Taken together, these factors position BFO@NCQDs as a cost-effective, scalable, and environmentally sustainable electrode material with strong potential for commercial supercapacitor applications.

6. Conclusion

A simple hydrothermal technique was employed to fabricate homogeneous magnetic nanocomposites containing nitrogen-doped carbon quantum dots (BFO@NCQDs). BET analysis revealed that BFO@NCQDs possess an excellent specific surface area of 821.65 m^2/g. Analysis of BFO@NCQDs' crystal structure, elemental content, and morphology was carried out with the use of XRD, XPS, FTIR, FE-SEM, and HR-TEM. The produced BFO@NCQDs magnetic nanocomposites exhibited magnetic characteristics, with a *Ms* of approximately 50.59 emu/g. NCQDs were found to significantly influence BFO's size, crystallinity, and thickness, acting as effective structure-directing agents. When employed as electrode materials for supercapacitors, BFO@NCQDs demonstrated an enhanced specific capacitance *Cs* of ~1513.94 F/g at 5 mV/s, as determined by CV in a 5 M KOH electrolyte. GCD studies further confirmed improved capacitive performance, yielding a *Cs* of 1984.98 F/g at an I_d of 2 A/g. The improved performance of the capacitor is attributed to the distinctive characteristics and diminutive size of NCQDs. In particular, the BFO@NCQDs-based symmetric cell exhibits a high power density (P_t) of 2090.39 W/kg and an energy density (E_t) of about 42.805 Wh/kg. However, when the P_t was 7565.43 W/kg, the E_t dropped to 17.018 Wh/kg, and the cycling stability was outstanding, with 91.1 % retention after 10,000 cycles at 12 A/g. These results highlight BFO@NCQDs magnetic nanocomposites as a cost-effective, eco-friendly, and readily manufacturable electrode material with superior conductivity. This material is a viable contender for electrochemical supercapacitors in energy storage applications and can also serve as a reliable backup power supply for portable electronic devices.

CRediT authorship contribution statement

Basheer M. Al-Maswari: Writing – review & editing, Writing – original draft, Validation, Methodology, Investigation, Formal analysis, Data curation, Conceptualization. **Eman Ramadan Elsharkawy:** Writing – review & editing, Visualization, Resources, Project administration, Funding acquisition, Formal analysis. **Awatif Rashed Z. Almotairy:** Writing – review & editing, Validation, Software, Resources, Investigation, Formal analysis. **Khaled Alkanad:** Writing – review & editing, Visualization, Validation, Methodology, Investigation, Formal analysis. **Abdelkader Zarrouk:** Writing – review & editing, Visualization, Validation, Resources. **Fatima A.S. Al-Yusufy:** Writing – review & editing, Visualization, Formal analysis. **B.M. Venkatesha:** Writing – review & editing, Visualization, Supervision, Resources.

Declaration of competing interest

The authors declare that they have no known competing financial interests or personal relationships that could have appeared to influence the work reported in this paper.

Acknowledgment

Basheer M. Al-Maswari is thankful to Amran University, Amran, Yemen, and the University of Mysore, Mysore, India. The authors extend their appreciation to Northern Border University, Saudi Arabia, for supporting this work through project number (NBU-CRP-2025-249).

Data availability

Data will be made available on request.

References

[1] J. Xiao, R. Momen, C. Liu, Application of carbon quantum dots in supercapacitors: a mini review, Electrochem. Commun. 132 (2021) 107143.
[2] P. Cai, R. Momen, M. Li, Y. Tian, L. Yang, K. Zou, et al., Functional carbon materials processed by NH_3 plasma for advanced full-carbon sodium-ion capacitors, Chem. Eng. J. 420 (2021) 129647.
[3] K. Zou, P. Cai, X. Deng, B. Wang, C. Liu, J. Li, et al., Revealing dual capacitive mechanism of carbon cathode toward ultrafast quasi-solid-state lithium ion capacitors, J. Energy Chem. 60 (2021) 209–221.
[4] X. Deng, K. Zou, R. Momen, P. Cai, J. Chen, H. Hou, et al., High content anion (S/se/P) doping assisted by defect engineering with fast charge transfer kinetics for high-performance sodium ion capacitors, Sci. Bull. 66 (2021) 1858–1868.
[5] B.M. Al-Maswari, N. Al-Zaqri, J. Ahmed, T. Ahamad, A. Boshaala, S. Ananda, et al., Nanomagnetic strontium ferrite nitrogen doped carbon ($SrFe_2O_4$-NC): synthesis, characterization and excellent supercapacitor performance, J Energy Storage 52 (2022) 104821.
[6] T.A. Manfo, H. Laaksonen, A review of carbon-based hybrid materials for supercapacitors, New Carbon Mater. 40 (2025) 81–110.
[7] K. Munir, G. Nabi, Cobalt substitution impact on structural modifications and capacitive contributions of $BiVO_4$ nanorods for promising pseudocapacitors electrode applications, Mater. Sci. Eng. B 317 (2025) 118199.
[8] M. El-Alouani, O. Kharbouch, K. Dahmani, N. Errahmany, I. Saber, M. Galai, et al., Enhancing Al–air battery performance with beta-D-glucose and adonite additives: a combined electrochemical and theoretical study, Langmuir 41 (2025) 431–449.
[9] M. Zhang, L. He, T. Shi, R. Zha, Nanocasting and direct synthesis strategies for mesoporous carbons as supercapacitor electrodes, Chem. Mater. 30 (2018) 7391–7412.
[10] B.M. Al-Maswari, N. Al-Zaqri, K. Alkanad, F.H. AlOstoot, A. Boshaala, R. T. Radhika, et al., Magnesium bismuth ferrite nitrogen-doped carbon nanomagnetic perovskite: synthesis and characterization as a high-performance electrode in a supercapacitor for energy storage, ACS Omega 8 (2023) 16145–16157.
[11] B.M. Al-Maswari, J. Ahmed, N. Alzaqri, T. Ahamad, Y. Mao, A. Hezam, et al., Synthesis of perovskite bismuth ferrite embedded nitrogen-doped carbon ($BiFeO_3$-NC) nanocomposite for energy storage application, J Energy Storage 44 (2021) 103515.
[12] F.A. Permatasari, M.A. Irham, S.Z. Bisri, F. Iskandar, Carbon-based quantum dots for supercapacitors: recent advances and future challenges, Nanomaterials 11 (2021) 91.
[13] Y. Liu, W. Li, P. Wu, C. Ma, X. Wu, M. Xu, et al., Hydrothermal synthesis of nitrogen and boron co-doped carbon quantum dots for application in acetone and dopamine sensors and multicolor cellular imaging, Sensors Actuators B Chem. 281 (2019) 34–43.
[14] M. Li, T. Chen, J.J. Gooding, J. Liu, Review of carbon and graphene quantum dots for sensing, ACS Sensors 4 (2019) 1732–1748.

[15] A. Dager, T. Uchida, T. Maekawa, M. Tachibana, Synthesis and characterization of mono-disperse carbon quantum dots from fennel seeds: photoluminescence analysis using machine learning, Sci. Rep. 9 (2019) 14004.
[16] Y. Vyas, P. Chundawat, D. Dharmendra, A. Jain, P.B. Punjabi, C. Ameta, Biosynthesis and characterization of carbon quantum dots@CuS composite using water hyacinth leaves and its usage in photocatalytic dilapidation of brilliant green dye, Mater. Chem. Phys. 281 (2022) 125921.
[17] P. Kumar, S. Dua, R. Kaur, M. Kumar, G. Bhatt, A review on advancements in carbon quantum dots and their application in photovoltaics, RSC Adv. 12 (2022) 4714–4759.
[18] A. Aouadi, D.H. Saoud, A. Bouafia, H.A. Mohammed, H.G. Gamal, A. Achouri, et al., Unveiling the antioxidant power: synthesis and characterization of lemon and orange peel-derived carbon quantum dots with exceptional free radical scavenging activity, Biomass Convers. Biorefinery 15 (2025) 9691–9704.
[19] C. Cheng, Q. Liang, M. Yan, Z. Liu, Q. He, T. Wu, et al., Advances in preparation, mechanism and applications of graphene quantum dots/semiconductor composite photocatalysts: a review, J. Hazard. Mater. 424 (2022) 127721.
[20] Q. Xu, Y. Niu, J. Li, Z. Yang, J. Gao, L. Ding, et al., Recent progress of quantum dots for energy storage applications, Carbon Neutrality 1 (2022) 13.
[21] Y. Liu, C. Liu, C. Shi, W. Sun, X. Lin, W. Shi, et al., Carbon-based quantum dots (QDs) modified ms/tz-$BiVO_4$ heterojunction with enhanced photocatalytic performance for water purification, J. Alloys Compd. 881 (2021) 160437.
[22] H. Feng, J. Liu, Y. Mu, N. Lu, S. Zhang, M. Zhang, et al., Hybrid ultrafiltration membranes based on PES and MOFs@carbon quantum dots for improving anti-fouling performance, Sep. Purif. Technol. 266 (2021) 118586.
[23] M. Nasrollahzadeh, M. Sajjadi, S. Iravani, R.S. Varma, Carbon-based sustainable nanomaterials for water treatment: state-of-art and future perspectives, Chemosphere 263 (2021) 128005.
[24] S. Zahmatkesh, B.-J. Ni, J.J. Klemeš, A. Bokhari, M. Hajiaghaei-Keshteli, Carbon quantum dots-ag nanoparticle membrane for preventing emerging contaminants in oil produced water, J Water Process Eng 50 (2022) 103309.
[25] Y. Vyas, P. Chundawat, D. Dharmendra, P.B. Punjabi, C. Ameta, Review on hydrogen production photocatalytically using carbon quantum dots: future fuel, Int. J. Hydrog. Energy 46 (2021) 37208–37241.
[26] Y. Vyas, P. Chundawat, P. Dharmendra, C. Ameta, Green and facile synthesis of luminescent CQDs from pomegranate peels and its utilization in the degradation of azure B and amido black 10B by decorating it on CuO nanorods, ChemistrySelect 6 (2021) 8566–8580.
[27] M.Y. Kalashgrani, F.F. Nejada, V. Rahmanianb, Carbon quantum dots platforms: as nano therapeutic for biomedical applications, luminescence 32 (2022) 33.
[28] V. Manikandan, N.Y. Lee, Green synthesis of carbon quantum dots and their environmental applications, Environ. Res. 212 (2022) 113283.
[29] M.E. Khan, A. Mohammad, T. Yoon, State-of-the-art developments in carbon quantum dots (CQDs): photo-catalysis, bio-imaging, and bio-sensing applications, Chemosphere 302 (2022) 134815.
[30] S. Santiago, T.N. Lin, C.-H. Chang, Y.-A. Wong, C.-A.J. Lin, C.-T. Yuan, et al., Synthesis of N-doped graphene quantum dots by pulsed laser ablation with diethylenetriamine (DETA) and their photoluminescence, Phys. Chem. Chem. Phys. 19 (2017) 22395–22400.
[31] S. Kang, Y.K. Jeong, J.H. Ryu, Y. Son, W.R. Kim, B. Lee, et al., Pulsed laser ablation based synthetic route for nitrogen-doped graphene quantum dots using graphite flakes, Appl. Surf. Sci. 506 (2020) 144998.
[32] M. Mubasher, H. Mumtaz, B. Nazir, S. Ullah Hussain, M. Ali, AC-conduction mechanism in SiO_2-coated $BaFe_2O_4$ nanoparticles, Applied Physics A 128 (2022) 285.
[33] G. Singh, S. Chandra, Electrochemical performance of $MnFe_2O_4$ nano-ferrites synthesized using thermal decomposition method, Int. J. Hydrog. Energy 43 (2018) 4058–4066.
[34] V. Deshmukh, H. Harini, R. Naik, H. Nagaswarupa, N. Basavaraju, B.A. Al-Asbahi, et al., Enhanced multifunctional properties of lanthanum-doped barium ferrite nanoparticles synthesized via sol-gel assisted hydrothermal method, J Energy Storage 82 (2024) 110559.
[35] U. Naresh, R.J. Kumar, N. Gupta, D. Kothandan, Ferroelectric properties of $CuFe_2O_4$, $BaFe_2O_4$, $Ba_{0.2}La_{0.8}Fe_2O_4$ nanoparticles, Electrical Sci. Eng. 1 (2019) 28–33.
[36] S. Majetich, J. Scott, E. Kirkpatrick, K. Chowdary, K. Gallagher, M. McHenry, Magnetic nanoparticles and magnetocrystalline anisotropy, Nanostruct. Mater. 9 (1997) 291–300.
[37] A.R.Z. Almotairy, B.M. Al-Maswari, K. Alkanad, N. Lokanath, R. Radhika, B. Venkatesha, Nickel vanadate nitrogen-doped carbon nanocomposites for high-performance supercapacitor electrode, Heliyon 9 (2023).
[38] B.M. Al-Maswari, E.R. Elsharkawy, A.R.Z. Almotairy, K. Alkanad, F.A. Al-Yusufy, A. Zarrouk, et al., Synthesis and characterization of a nanocomposite electrode of titanium ferrite N-doped carbon for high-performance supercapacitor applications, Inorg. Chem. Commun. 179 (Part 2) (2025) 114890.
[39] S. Wang, H. Gao, G. Sun, J. Zhang, Y. Xia, C. Xie, et al., M-type barium hexaferrite nanoparticles synthesized by γ-ray irradiation assisted polyacrylamide gel method and its optical, magnetic and supercapacitive performances, J. Clust. Sci. 32 (2021) 569–578.
[40] H. Wang, Y. Xu, L. Jing, S. Huang, Y. Zhao, M. He, et al., Novel magnetic $BaFe_{12}O_{19}$/g-C_3N_4 composites with enhanced thermocatalytic and photo-Fenton activity under visible-light, J. Alloys Compd. 710 (2017) 510–518.
[41] M. Naushad, T. Ahamad, B.M. Al-Maswari, A.A. Alqadami, S.M. Alshehri, Nickel ferrite bearing nitrogen-doped mesoporous carbon as efficient adsorbent for the removal of highly toxic metal ion from aqueous medium, Chem. Eng. J. 330 (2017) 1351–1360.
[42] B. Vercelli, R. Donnini, F. Ghezzi, A. Sansonetti, U. Giovanella, B. La Ferla, Nitrogen-doped carbon quantum dots obtained hydrothermally from citric acid and urea: the role of the specific nitrogen centers in their electrochemical and optical responses, Electrochim. Acta 387 (2021) 138557.
[43] K. Yokwana, B. Ntsendwana, E.N. Nxumalo, S.D. Mhlanga, Recent advances in nitrogen-doped graphene oxide nanomaterials: synthesis and applications in energy storage, sensor electrochemical applications and water treatment, J. Mater. Res. 38 (2023) 3239–3263.
[44] J. Yan, R. Sun, L. Shen, H. Bai, S. Jiang, Y. Xiao, et al., Hydrogen-rich syngas production with tar elimination via biomass chemical looping gasification (BCLG) using $BaFe_2O_4/Al_2O_3$ as oxygen carrier, Chem. Eng. J. 387 (2020) 124107.
[45] I.S. Khan, I.H. Gul, Comparative investigation of magnetic, di-electric, optical, and electrical properties of mono-$BaFe_2O_4$ and hexa-$BaFe_{12}O_{19}$ nano-ferrites for photovoltaic (PV) applications, Applied Physics A 128 (2022) 1109.
[46] T. Ahamad, M. Naushad, S.I. Al-Saeedi, S.M. Alshehri, N/S-doped carbon embedded with AgNPs as a highly efficient catalyst for the reduction of toxic organic pollutants, Mater. Lett. 264 (2020) 127310.
[47] T. Ahamad, M. Naushad, B.M. Al-Maswari, S.M. Alshehri, Fabrication of highly porous adsorbent derived from bio-based polymer metal complex for the remediation of water pollutants, J. Clean. Prod. 208 (2019) 1317–1326.
[48] O.M.K. Koç, A.E. Üzer, R.A. Apak, High quantum yield nitrogen-doped carbon quantum dot-based fluorescent probes for selective sensing of 2, 4, 6-trinitrotoluene, ACS Appli. Nano Mater. 5 (2022) 5868–5881.
[49] A. Amasegowda, K. Alkanad, N. Al-Zaqri, A. Al-khawlani, A.U. Kumar, B.M. Al-Maswari, et al., Boosted photocatalytic H_2 production over pn S-scheme heterojunction of 0D $Ni_3V_2O_8$ quantum dots decorated on ultra-thin 2D g-C_3N_4 nanosheets, J. Environ. Chem. Eng. 12 (2024) 111841.
[50] T. Narkbuakaew, P. Sujaridworakun, Synthesis of tri-s-triazine based gC_3N_4 photocatalyst for cationic rhodamine B degradation under visible light, Top. Catal. 63 (2020) 1086–1096.
[51] T. Ahamad, $CoSe_2$@N-doped graphene nanocomposite high-efficiency counter electrode for dye-sensitized solar cells, J. Inorg. Organomet. Polym. Mater. (2022) 1–10.
[52] M.O. Amin, B. D'Cruz, E. Al-Hetlani, Continuous synthesis of $BaFe_2O_4$ and $BaFe_{12}O_{19}$ nanoparticles in a droplet microreactor for efficient detection of antihistamine drugs in oral fluid using surface-assisted laser desorption/ionization mass spectrometry, Analyst 148 (2023) 4489–4503.
[53] M. Verma, A.P. Singh, P. Sambyal, B.P. Singh, S. Dhawan, V. Choudhary, Barium ferrite decorated reduced graphene oxide nanocomposite for effective electromagnetic interference shielding, Phys. Chem. Chem. Phys. 17 (2015) 1610–1618.
[54] R. Dilip, R. Jayaprakash, P. Sangaiya, S. Gopi, The magnetic property alterations due to transition from barium ferrite ($BaFe_2O_4$) nano rods to barium carbonate ($BaCO_3$) quantum dots, Res. Mater. 7 (2020) 100121.
[55] M.N. Akhtar, M.A. Khan, Effect of rare earth doping on the structural and magnetic features of nanocrystalline spinel ferrites prepared via sol gel route, J. Magn. Magn. Mater. 460 (2018) 268–277.
[56] I. Ahmad, S.M. Shah, M.N. Zafar, M.N. Ashiq, W. Tang, U. Jabeen, Synthesis, characterization and charge transport properties of Pr–NiCo-doped $SrFe_2O_4$ spinel for high frequency devices applications, Ceram. Int. 47 (2021) 3760–3771.
[57] A. Abdalazeez, T. Li, X. Liu, Y. Cao, W. Wang, S. Abuelgasim, et al., Investigation of $BaFe_2O_4$ oxygen carrier modified by supports in chemical looping gasification of biochar, Int. J. Hydrog. Energy 49 (2024) 238–251.
[58] M. Casappa, F. Pattini, G. Spaggiari, F. Mezzadri, S. Rampino, Growth of multiferroic γ-$BaFe_2O_4$ thin films by pulsed Electron deposition technique, J. Alloys Compd. 987 (2024) 174193.
[59] E. Ahilandeswari, K. Sakthipandi, R.R. Kanna, M. Hubálovská, D. Vigneswaran, Lanthanum substitution effect on the structural, optical, and dielectrical properties of nanocrystalline $BaFe_2O_4$ ferrites, Phys. B Condens. Matter 635 (2022) 413849.
[60] R. Sikkema, I. Zhitomirsky, Magnetic supercapacitors: Charge storage mechanisms, magnetocapacitance, and magnetoelectric phenomena, Appl. Phys. Rev. vol. 10 (2023).
[61] X. Li, L. Zhang, H. Liu, Q. Li, Y. Hou, Magnetic measurements applied to energy storage, Adv. Energy Mater. 13 (2023) 2300927.
[62] S.R. Ka, C.S. Rout, Recent developments, challenges and future prospects of magnetic field effects in supercapacitors, J Mater Chem A 11 (2023) 5495–5519.
[63] M. Wang, K. An, Y. Fang, G. Wei, J. Yang, L. Sheng, et al., The microwave absorbing properties of $CoFe_2$ attached single walled carbon nanotube/$BaFe_{12}O_{19}$ nanocomposites, J. Mater. Sci. Mater. Electron. 28 (2017) 12475–12483.
[64] R. Peymanfar, M. Rahmanisaghieh, A. Ghaffari, Y. Yassi, "Preparation and identification of $BaFe_2O_4$ nanoparticles by the sol–gel route and investigation of its microwave absorption characteristics at ku-band frequency using silicone rubber medium," in *Proceedings*, 2018, p. 5234.

[65] R.Y. Pawar, S.K. Pardeshi, Selective oxidation of styrene to benzaldehyde using soft $BaFe_2O_4$ synthesized by citrate gel combustion method, Arab. J. Chem. 11 (2018) 282–290.
[66] I. Ştefan, G.C. Benga, I.D. Savu, S.V. Savu, B.A. Olei, "Investigating the Effect of α-Fe_2O_3 Oxides on the $BaFe_2O_4$ Pyrosynthesis Temperature-the Digital Processing of TG and DTA Curves," in *Advanced Engineering* Forum, 2021, pp. 42–49.
[67] P.R. Kharangarh, N.M. Ravindra, R. Rawal, A. Singh, V. Gupta, Graphene quantum dots decorated on spinel nickel cobaltite nanocomposites for boosting supercapacitor electrode material performance, J. Alloys Compd. 876 (2021) 159990.
[68] S. Venkateswarlu, H. Mahajan, A. Panda, J. Lee, S. Govindaraju, K. Yun, et al., Fe_3O_4 nano assembly embedded in 2D-crumpled porous carbon sheets for high energy density supercapacitor, Chem. Eng. J. 420 (2021) 127584.
[69] L.S. Ghadimi, N. Arsalani, A.G. Tabrizi, A. Mohammadi, I. Ahadzadeh, Novel nanocomposite of $MnFe_2O_4$ and nitrogen-doped carbon from polyaniline carbonization as electrode material for symmetric ultra-stable supercapacitor, Electrochim. Acta 282 (2018) 116–127.
[70] A. Kumar, N. Kumar, Y. Sharma, J. Leu, T.Y. Tseng, Synthesis of free-standing flexible rGO/MWCNT films for symmetric supercapacitor application, Nanoscale Res. Lett. 14 (2019) 1–17.
[71] H. Yang, S. Kannappan, A.S. Pandian, J.-H. Jang, Y.S. Lee, W. Lu, Graphene supercapacitor with both high power and energy density, Nanotechnology 28 (2017) 445401.
[72] S. Sharifi, A. Yazdani, K. Rahimi, Incremental substitution of Ni with Mn in $NiFe_2O_4$ to largely enhance its supercapacitance properties, Sci. Rep. 10 (2020) 1–15.
[73] B.-A. Mei, O. Munteshari, J. Lau, B. Dunn, L. Pilon, Physical interpretations of Nyquist plots for EDLC electrodes and devices, J. Phys. Chem. C 122 (2018) 194–206.
[74] Y.-S. Lee, Y.A. Kumar, S. Sambasivam, S.A. Hira, K. Zeb, W. Uddin, et al., $CoCu_2O_4$ nanoflowers architecture as an electrode material for battery type supercapacitor with improved electrochemical performance, Nano-Struct. Nano-Objects 24 (2020) 100618.
[75] M. Chen, D. Yu, X. Zheng, X. Dong, Biomass based N-doped hierarchical porous carbon nanosheets for all-solid-state supercapacitors, J Energy Storage 21 (2019) 105–112.
[76] Q. Wu, T. He, Y. Zhang, J. Zhang, Z. Wang, Y. Liu, et al., Cyclic stability of supercapacitors: materials, energy storage mechanism, test methods, and device, J Mater Chem A 9 (2021) 24094–24147.
[77] Y. Wen, L. Chi, K. Wenelska, X. Wen, X. Chen, E. Mijowska, Eucalyptus derived heteroatom-doped hierarchical porous carbons as electrode materials in supercapacitors, Sci. Rep. 10 (2020) 14631.
[78] S. Yetiman, F.K. Dokan, M.S. Onses, E. Yilmaz, A.T. Ozdemir, E. Sahmetlioglu, Redox electrolyte mediated performance enhancement in aqueous zinc ion hybrid supercapacitors composed of spinel $BaFe_2O_4$ and cubic Cu_2O, J. Mater. Chem. C 12 (2024) 6865–6880.
[79] Z. Ji, N. Li, Y. Zhang, M. Xie, X. Shen, L. Chen, et al., Nitrogen-doped carbon dots decorated ultrathin nickel hydroxide nanosheets for high-performance hybrid supercapacitor, J. Colloid Interface Sci. 542 (2019) 392–399.
[80] M. Zhang, W. Liu, A. Yu, "Superior Micro-Supercapacitors Based on Graphenequantum Dots," in *Electrochemical Society Meeting Abstracts* 235, 2019, 956–956.
[81] H. Xia, C. Hong, B. Li, B. Zhao, Z. Lin, M. Zheng, et al., Facile synthesis of hematite quantum-dot/functionalized graphene-sheet composites as advanced anode materials for asymmetric supercapacitors, Adv. Funct. Mater. 25 (2015) 627–635.
[82] J. Luo, J. Wang, S. Liu, W. Wu, T. Jia, Z. Yang, et al., Graphene quantum dots encapsulated tremella-like $NiCo_2O_4$ for advanced asymmetric supercapacitors, Carbon 146 (2019) 1–8.
[83] G. Wei, X. Zhao, K. Du, Y. Huang, C. An, S. Qiu, et al., Flexible asymmetric supercapacitors made of 3D porous hierarchical $CuCo_2O_4$@CQDs and Fe_2O_3@CQDs with enhanced performance, Electrochim. Acta 283 (2018) 248–259.
[84] Y. Zhu, Z. Wu, M. Jing, H. Hou, Y. Yang, Y. Zhang, et al., Porous $NiCo_2O_4$ spheres tuned through carbon quantum dots utilised as advanced materials for an asymmetric supercapacitor, J Mater Chem A 3 (2015) 866–877.
[85] M. Naushad, T. Ahamad, M. Ubaidullah, J. Ahmed, A.A. Ghafar, K.M. Al-Sheetan, et al., Nitrogen-doped carbon quantum dots (N-CQDs)/Co_3O_4 nanocomposite for high performance supercapacitor, J. King Saud Univ. Sci. 33 (2021) 101252.
[86] Z. Li, J. Wei, J. Ren, X. Wu, L. Wang, D. Pan, et al., Hierarchical construction of high-performance all-carbon flexible fiber supercapacitors with graphene hydrogel and nitrogen-doped graphene quantum dots, Carbon 154 (2019) 410–419.
[87] Z. Ji, D. Ma, W. Dai, K. Liu, X. Shen, G. Zhu, et al., Anchoring nitrogen-doped carbon quantum dots on nickel carbonate hydroxide nanosheets for hybrid supercapacitor applications, J. Colloid Interface Sci. 590 (2021) 614–621.
[88] J. Kong, Y. Wei, F. Zhou, L. Shi, S. Zhao, M. Wan, et al., Carbon quantum dots: properties, preparation, and applications, Molecules 29 (2024) 2002.
[89] Z. Ikram, E. Azmat, M. Perviaz, Degradation efficiency of organic dyes on CQDs as photocatalysts: a review, ACS Omega 9 (2024) 10017–10029.
[90] J. Guzmán-Mínguez, V. Fuertes, C. Granados-Miralles, J. Fernández, A. Quesada, Greener processing of $SrFe_{12}O_{19}$ ceramic permanent magnets by two-step sintering, Ceram. Int. 47 (2021) 31765–31771.

Basheer M. Al-Maswari, is serving as Assistant Professor at Department of Chemistry, Faculty of Applied Sciences and Humanities, Amran University, Yemen since end of 2024 to now. Received Ph.D. in Chemistry 2024 Department of Chemistry, Yuvaraja's College, University of Mysore, India under supervisor prof B.M. Venkatesha. M.Sc. in Chemistry (2018) Department of Chemistry, Faculty of Science, King Saud University, Riyadh, Saudi Arabia. B.Sc. in Chemistry (2007) Faculty of Science, Sana'a University, Yemen. B.Sc. in Chemistry (2004) Faculty of Education, Sana'a University, Yemen. His researches focuses on ferrite nanocomposite and their various applications, including ferroelectric and magnetic composites, with the aim of developing environmentally friendly magnetoelectric devices, supercapacitors, perovskite solar cells, and electrodes for renewable energy storage. He also explores the applications of ferrites in wastewater treatment and the removal of highly toxic heavy metals from aqueous solutions. And published 41 research publications in international journals of high repute. He works as a reviewer in many scientific journals such as (Environmental Chemical Engineering, Ions, Chemistry Select, Hindawi). Received the best researcher award at Amran University in the AD SCIENTIFIC INDEX 2025, 2026 global ranking in scientific research for the years 2025 and 2026. Received a gold medal and certificate as the Best International Researcher in Sustainable Energy (Supercapacitors and Energy Storage) from the ISSN 2022 International Research Awards held in India in 2022. Received the Best Poster Presentation Award from the International Winter School on Horizons in Materials Science, Jawaharlal Nehru Centre for Advanced Scientific Research, Bengaluru, India (2022). Won first place in the Pure Science Competition at the College of Science and Department of Chemistry level during my participation in the 2018 Scientific Research Forum held at the College of Science, King Saud University (best published research at the College of Science level).

Eman Ramadan Elsharkawy, Asc. Prof in Organic chemistry (Natural Product chemistry). Earned, master's and PhD degree in Organic chemistry, Ph.D. from Ain Shamus University, Egypt. I am worked for 9 years as supervisor of chemistry Department Arar branch, girl section, Northern Border University, currently working as an Associate Professor in the Centre of Health Research, Northern Border University, Saudi Arabia. I have published more than 75 research papers, with international publishers, I am a member of different scientific bodies and a reviewer of journals of national and international repute. My research focuses on Natural Product Chemistry, Phytochemistry Including Isolation, Purification and Structural Elucidation of the Different Classes of Natural Products which isolated from Medicinal, Terrestrial Plants and Marine sources., Computational Phytochemistry, Biological evaluation of the extracts, fractions and the isolates: (anticancer, antidiabetic, Antiviral and Antialzheimer). According to Vision of university, Present study concern on the effect of environmental conditions including climatic change on the bioactive compounds and application of the desert plants and compound isolated. In addition to research interests in obtaining environmentally friendly electrical energy from renewable sources by storing it in electrodes such as supercapacitors. i, actively collaborates with academic and research partners and has been recognized for his contributions to the field through research initiatives and scholarly publications.

Awatif Rashed Z. Almotairy, has currently serves as associated Professor at Taibah University, Yanbu, kingdom of Saudi Arabia. She has been part of the Taibah faculty since 2020 and brings with her over five years of rich teaching experience. Throughout this academic work, she has mentored students at various academic levels and has successfully supervised many theses. She has authored more than 30 research papers published in international journals indexed in the Science Citation Index (SCI) and Science Citation Index Expanded (SCIE), along with several conference proceedings. Her scientific group was awarded research funding by the Deputyship for Research and Innovation, Ministry of Education, Saudi Arabia, through project number 442/56, in recognition of them outstanding research proposal. Her current work focuses on the effective utilization of renewable energy sources by storing them in supercapacitors, synthesizing engineered nanomaterials as high-performance electrode components. Moreover, she explores the design of functional materials with biomedical relevance, including the role of metalloproteins with antioxidant and antimicrobial properties, nanostructures for targeted drug delivery, and environmentally responsive coordination compounds to bridge fundamental chemistry with real-world health and environmental applications.

Khaled Alkanad, obtained his Ph.D. in Physics from the University of Mysore, India, with a focus on the synthesis and characterization of semiconductor nanoheterostructures for photocatalytic applications. His research interests include advanced materials for energy storage and conversion, and environmental remediation, particularly in photocatalytic CO_2 reduction, water splitting, and pollutant degradation. Has published extensively in high-impact journals and has filed patents related to photocatalysis. He is a recipient of the prestigious Marie Skłodowska-Curie Postdoctoral Fellowship under the 2024 Horizon Europe call and was previously awarded a Seal of Excellence by the European Commission. He also serves as a reviewer for several international journals in inorganic chemistry and materials science.

Abdelkader Zarrouk, was born in 1973 in Taza, Morocco. He obtained his PhD in Physical-Chemistry of Materials from the Faculty of Sciences, Mohammed Premier University, Oujda, Morocco in 2011. He has published over 710 articles in international journals (indexed by Scopus) with an h-index = 87 (21083 citations according to Scopus); Google Scholar h-index = 89 (23638 citations according to Google Scholar) and has presented around 300 communications at symposia and national/international meetings. He has developed three Moroccan and six American patents. He is on the editorial board of twenty-six (26) international journals and has participated in the review of more than 500 articles in over 80 international journals published by Elsevier, Springer, the Royal Society of Chemistry, the American Chemical Society, Taylor and Francis and others. He is the author of two books and co-author of several book chapters (14). He is one of the top 2% of the world's most influential researchers (2020-2024) according to the Stanford University rankings. In 2021, he was awarded the Prize of Distinction at the 2nd Research Excellence Awards (best chemistry publisher), organised by the National Centre for Scientific and Technical Research (NCSTR) and Clarivate, on 29 June in Rabat, Morocco. In 2022, he was honoured with the Award of Distinction at the 1st edition of the 'Morocco Scopus Awards' in the field of materials science, organised by the NCSTR and ELSEVIER, on 6 October in Rabat, Morocco. He was ranked first in the Top 15 most prolific Moroccan researchers for the period 2014-2023 in chemistry according to Scopus data. His main research interests lie in the field of physical chemistry, particularly electrochemistry (corrosion and inhibition of metals and alloys). He is also interested in the application of certain quantum chemical methods such as density functional theory (DFT), molecular dynamics simulation and other semi-empirical methods. He is particularly interested in the elimination of heavy metals and radioactive elements using adsorbent materials, and his research focuses on organic solar cells, applications of newly developed thin films and the electro-fenton process.

Fatima A.S. Al-Yusufy, an associate professor in Organic chemistry, and I was awarded my BSc degree (1989), M.Sc (1997) and PhD (2000) in conducting polymers from the Department of Chemistry, Faculty of Science, Sana'a University, Sana'a, Yemen. I'm a Yemeni national and have been working as an academic staff member at Qassim University, Department of Chemistry, College of Science, Buraydah, Ar Rass branch, Saudi Arabia, since 2014. Most of my publications were mainly in conducting polymers, chelating polymers, and lately, nanomaterials, ferrite nanomaterials, and renewable energy. I have supervised several master's theses and acted as an external examiner in MSc and PhD theses of several postgraduate students. I have also acted as a reviewer of several publications in my professional experience.

B.M. Venkatesha, is a Professor of Chemistry at Yuvaraja's College, University of Mysore, Mysore, India. He has over 33 years of teaching experience at various levels, including B.Sc. and M.Sc. He has supervised four M.Phil. and five Ph.D. degrees. He has published over 55 research papers in internationally recognized journals, listed in the Science Citation Index. His research is prominent at the Center for Chemical Kinetics. He has presented over 30 research papers at seminars and conferences. His research focuses on reaction kinetics, production and characterization of biodiesel, pharmaceutical analysis, and the synthesis and characterization of nanomaterials, particularly in electrochemistry (supercapacitors and energy storage).